Hindawi Publishing Corporation
Science and Technology of Nuclear Installations
Volume 2012, Article ID 785157, 15 pages
doi:10.1155/2012/785157

Research Article

Experimental Investigation of Rising Gas Bubble Characteristics from a Vertical Tube under CCFL Condition

Kunihito Matsumura and Fumito Kaminaga

Faculty of Engineering, Ibaraki University, 4-12-1 Nakanarusawa, Hitachi Ibaraki 316-8511, Japan

Correspondence should be addressed to Kunihito Matsumura, kunimatsu@mx.ibaraki.ac.jp

Received 11 November 2011; Accepted 10 January 2012

Academic Editor: Michio Murase

This paper describes an experimental study of gas/liquid countercurrent flow in a vertical circular tube. CCFL experiments were carried out with three different water levels in the upper plenum, two different tube diameters. Measurements were made for liquid and gas flow rates, time variations of pressure at locations of the upper entry of the tube and lower plenum. Visual observations were also conducted to investigate the relationship between rising gas bubble characteristics and time variation of gas pressure at the upper entry of the tube. The results indicate that one bubble formation cycle (e.g., bubble growth, expansion, and detachment into the water pool) corresponds to one pressure fluctuation cycle. For the 20 mm diameter tube, it was confirmed that there was a characteristic waiting time between bubble cycles in which no bubble was formed at the upper entry of the tube. The waiting time is a favorable time for a liquid introduction into the tube from the upper plenum. The bubble volumes are compared with existing bubble formation correlations.

1. Introduction

Countercurrent gas/liquid flow is generally characterized by an interaction between a gas flowing upwards inside a conduit and a liquid falling counter-currently along its wall. It has been an important design criterion in a variety of industrial equipments, such as chemical reaction in a chemical reactor, evaporators, reflux condensers, and two phase heat exchangers. The departure from stable countercurrent gas/liquid flow is of major importance in the operation of Emergency Core Cooling System (ECCS) during a postulated loss of coolant accident in light water nuclear reactor. There is a possibility that the downward flow of emergency coolant may be limited by uprising steam generated from coolant evaporation, therefore, accurate prediction of CCFL is a significant aspect for evaluating the performance of core cooling devices. Countercurrent flow has been studied both experimentally and theoretically for a long time by many researchers. Although many studies have been made on the fundamental processes of the countercurrent flow, there is still some uncertainty about the precise mechanism in countercurrent flow transition.

The countercurrent flow transition can be classified into two regimes. One is generally called flooding which means the flow transition from the annular flow to the mixing flow occurred through an entire length of a flow channel and initiated by a large liquid entrainment due to choking of the gas flow path in the channel on increasing gas flow rate and/or liquid flow rate. The other is called the countercurrent flow limiting, CCFL, which occurs locally at an upper end of a channel connecting to a liquid pool besides a steady annular flow indicated on the other locations inside the channel. The most widely used empirical correlation for air/water countercurrent flow was proposed by Wallis [1]. This correlation derived from experiments in vertical small diameter tubes and it can be expressed as follows:

$$j_g^{*0.5} + m j_l^{*0.5} = C, \tag{1}$$

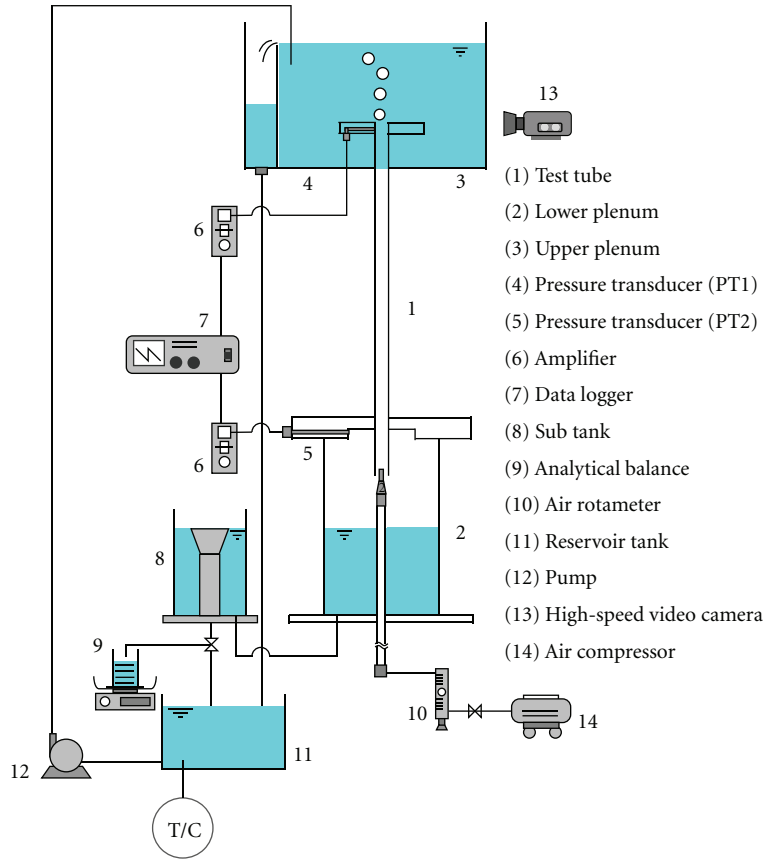

Figure 1: Schematic diagram of experimental apparatus.

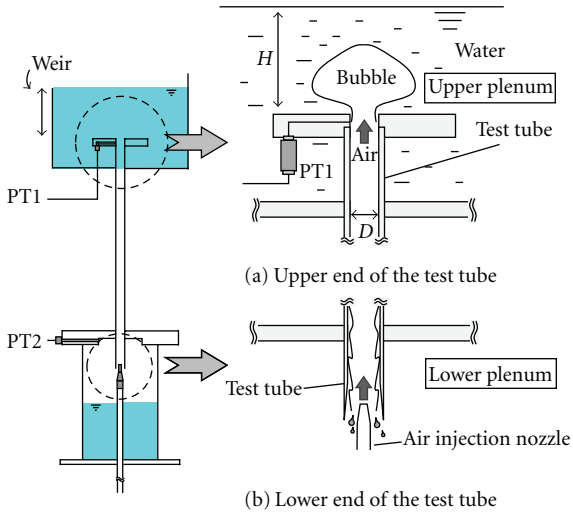

Figure 2: Details of the upper and lower end geometries.

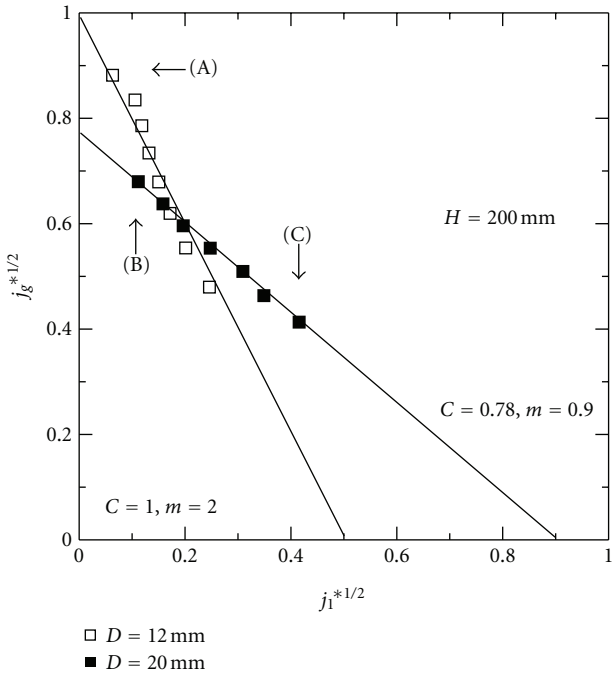

Figure 3: Dimensionless downward liquid flow rate against gas flow rate in CCFL condition for different tube diameter.

where j_g^* and j_l^* are the dimensionless gas and liquid superficial velocities given by

$$j_g^* = j_g \sqrt{\frac{\rho_g}{gD\left(\rho_l - \rho_g\right)}}, \tag{2}$$

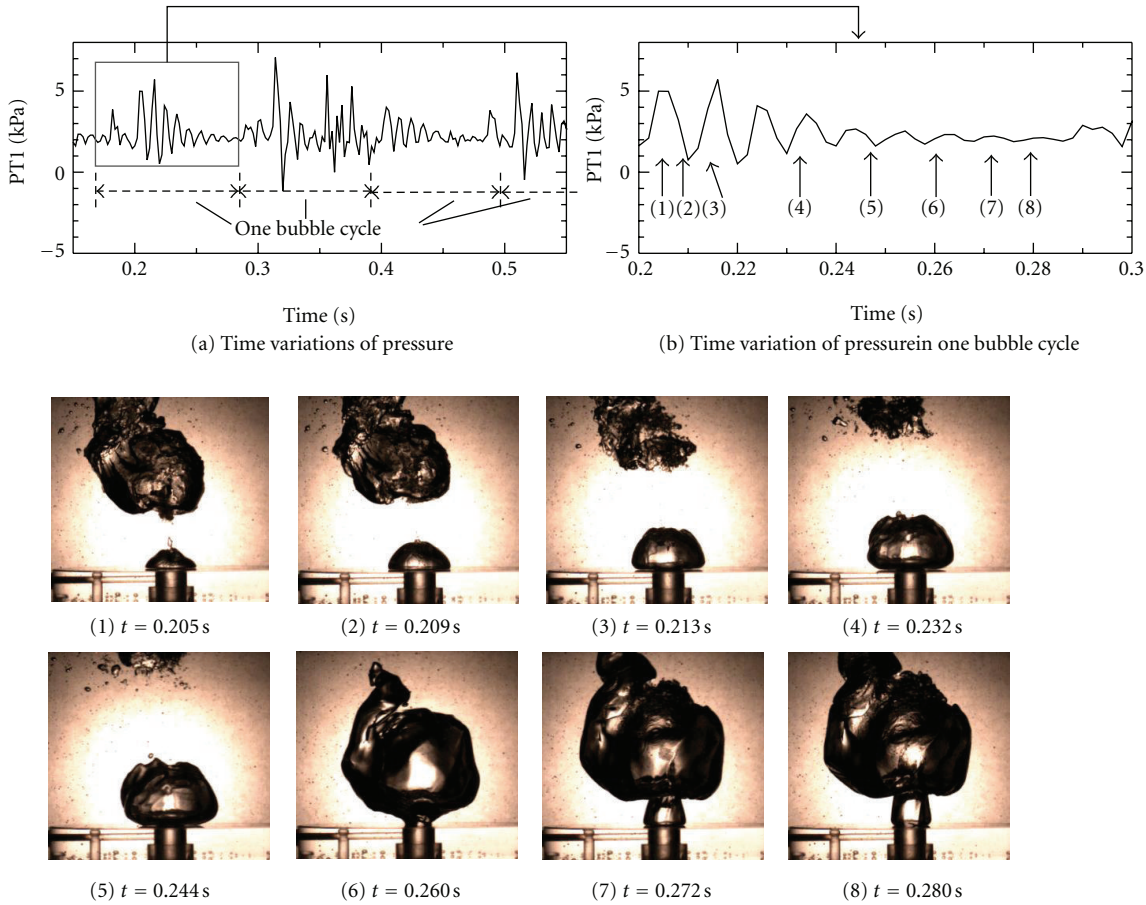

FIGURE 4: Time variations of pressure at the upper entry of the tube (PT1) and corresponding bubble formation and expansion process (tube diameter $D = 12$ mm, $j_g^{*0.5} = 0.88$, indicated as (a) in Figure 3).

$$j_l^* = j_l \sqrt{\frac{\rho_g}{gD\left(\rho_l - \rho_g\right)}}. \tag{3}$$

In (1), m and C are nondimensional constants which mainly depend on geometry, such as the liquid inlet and exit and tube diameter. In general, the value of m is equal to 1.0 approximately and the value of C lies between 0.6 to 1.0. Since most of the proposed correlations are not based on the physical mechanisms that cause flooding, a satisfactory correlation appreciable over a wide range of operating condition, fluid properties, and pipe geometry is still lacking. In addition, it is known that most analytical models used a forced balance equation for wall shear, interfacial shear, and gravity to determine a downward liquid flow rate flowing against an upward gas flow rate (Richter [2] and No and Jeong [3]). In the analysis, however, the interfacial shear force has a predominant effect on the predicted results and all established correlation for the interfacial shear were empirically obtained to be applicable to limited conditions. Therefore, even in update thermal-hydraulic computer codes like TRAC and RELAP, the Wallis-type empirical correlation is still used with the optional constant values, m and C, to predict downward liquid flow rate.

In a laboratory scale gas/liquid countercurrent flow experiments, typical equipments consist of upper and lower plenums connected by a vertical tube, in which liquid flow downward by gravity from the upper to the lower plenum. Gas is introduced into the lower plenum and flows upward counter-currently through the vertical tube. A pool of liquid in the upper plenum above the upper end of the tube provides the liquid penetrate into downward. Investigations using this experimental configuration include those of Kaminaga et al. [4], Imura et al. [5], Bharathan and Wallis [6], and Lu et al. [7]. In this experimental configuration, although the constant static head is kept in the upper plenum, the downward liquid flow rate is not generally kept constant. The downward liquid flow rate is influenced by not only flow behavior, such as interfacial shear or wall shear in the vertical tube but also bubble dynamics, such as bubble formation, growth, and departure at the upper end of the tube. Therefore, in order to predict countercurrent flow limit, it is important to clarify the relationship between rising

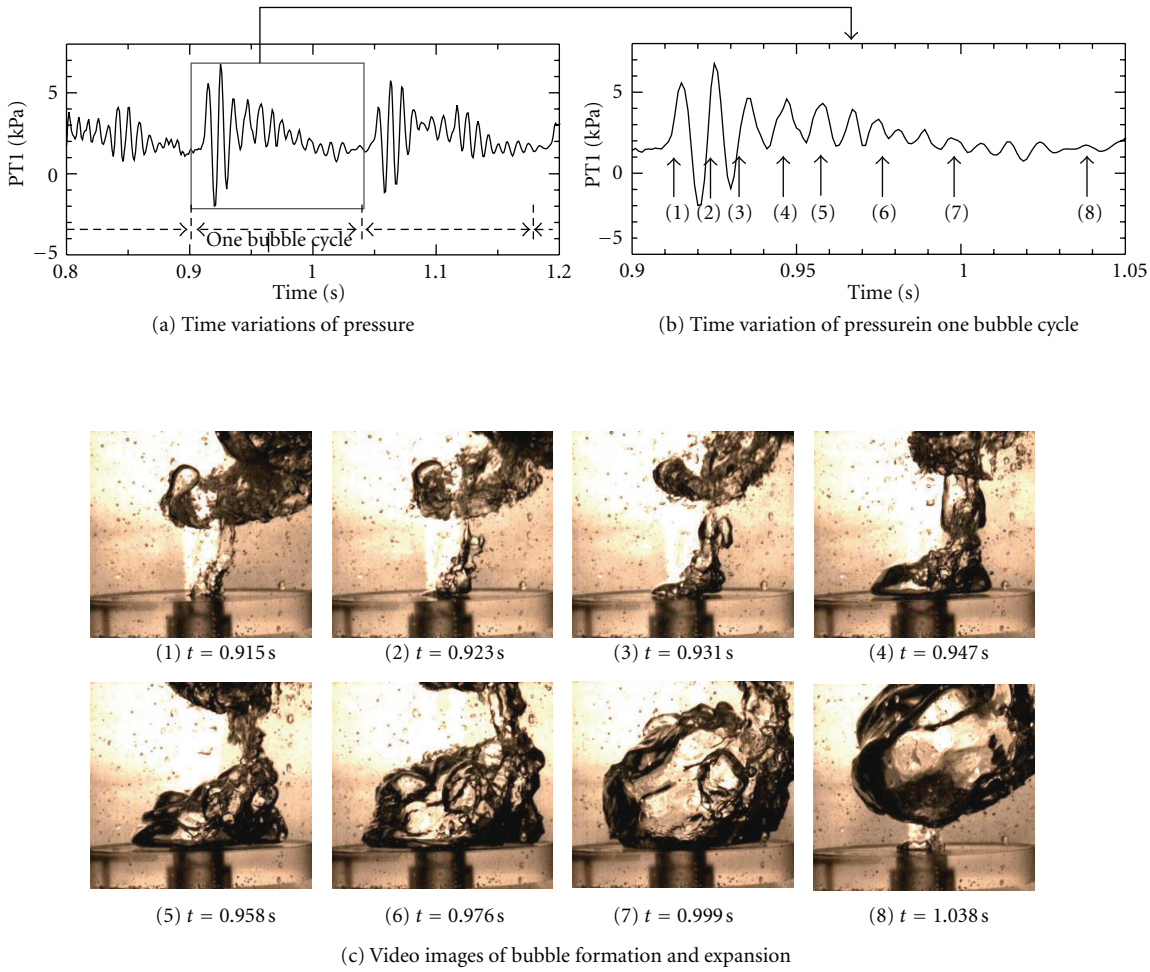

(a) Time variations of pressure

(b) Time variation of pressurein one bubble cycle

(c) Video images of bubble formation and expansion

FIGURE 5: Time variations of pressure at the upper entry of the tube (PT1) and corresponding bubble formation and expansion process (tube diameter D = 20 mm, $j_g^{*0.5}$ = 0.68, indicated as (b) in Figure 3).

bubble behavior at the upper end of the tube and downward liquid flow rate leading to flow transition.

Consequently, the purposes of this study are to experimentally examine adiabatic air/water countercurrent flow focusing on relationship between the downward liquid flow rate and behaviors of bubbles purged into the liquid pool. In this study, the experimental results from simultaneous measurements of the time variations of pressure inside the upper end of the tube and visual observations of bubble formation are presented.

2. Experimental Apparatus

A schematic diagram of the experimental apparatus is shown in Figure 1. It consists of a test tubean upper plenum, a lower plenuman air supply system, and data acquisition system. The test tube is made of circular transparent acrylic resin to facilitate visual observation and has a length of 1000 mm. The upper plenum (430 mm long, 320 mm wide, and 500 mm high) and the lower circular plenum (200 mm i.d. and 500 mm high) are interconnected by the vertical test tube. In order to examine the tube diameter effect on bubble formation, the tubes having 12 and 20 mm in diameter were used.

For the experiments, water at 293 K (±3 K) is pumped from a reservoir tank and is fed into the upper plenum. In the upper plenum, the water level was maintained to be constant by a weir and overflow water is fed back to the reservoir tank by gravity. The downward water flow rate through the vertical test tube was determined by collecting it in a measuring sub tank over a certain period of time. Air is directly fed to the lower plenum from the air compressor via a needle valve and air flow meter and allowed to flow upwards through the test tube.

Details of the upper and lower end geometries are shown in Figure 2. The upper end of the tube is sharp-edged geometry that a horizontal circular plate is attached at the end of the test tube. As shown in Figure 2(b), compressed air enters directly into the tapered tube bottom, through a small injection nozzle (i.d. = 4 mm) in the lower plenum. The injection nozzle is aligned accurately with the center of the vertical test tube. This air entrance section is designed to

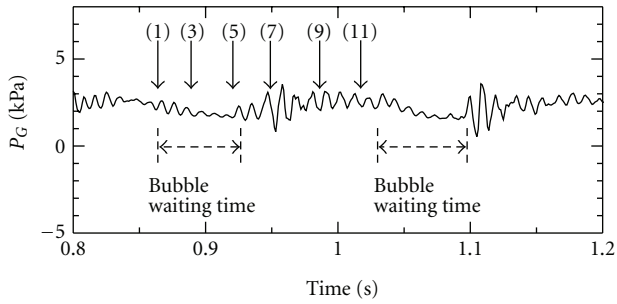

(a) Time variations of pressure

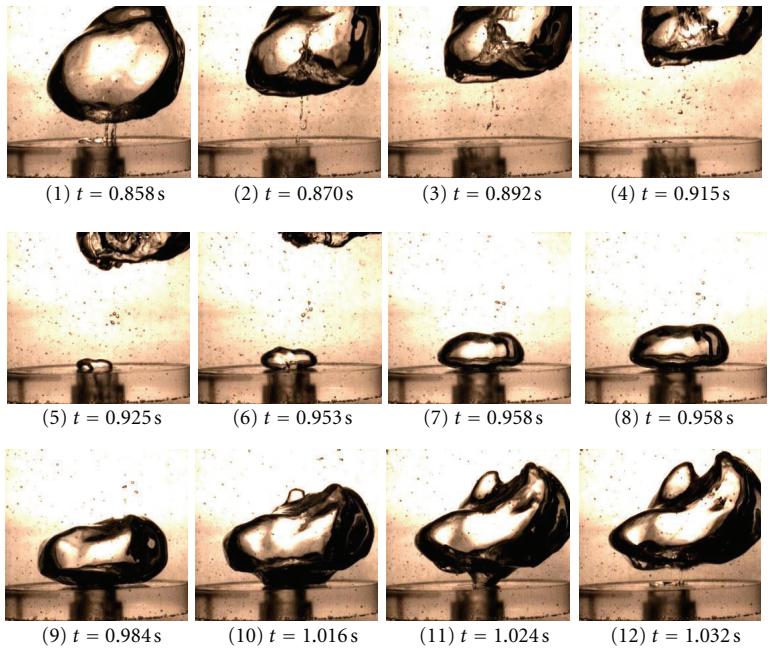

(b) Video images of bubble formation and expansion

Figure 6: Time variations of pressure at the upper entry of the tube (PT1) and bubble formation and expansion process including waiting time (tube diameter D = 20 mm, $j_g^{*0.5}$ = 0.41, indicated as (c) in Figure 3).

minimize the interaction between the falling water and the air near the lower end and make the flow controlled only by the flow behavior near the upper entry of the tube. The air supplied from the bottom injection nozzle goes up in the tube with a countercurrent flow regime and purged into the water pool with a large bubble regime. The water level is varied from 50 mm to 200 mm to examine an effect of the water level on a downward liquid flow rate in the CCFL condition. The water level in the upper plenum was controlled by the height of weir. In the present experiment, three different heights of weirs were used.

In each experiment, initially some amount of air only flows in the test section and then the water level in the upper plenum is set at a specified level to make a steady state countercurrent flow in the test section. During the steady-state, the air and downward water flow rates, the pressure at the upper entry of the tube (PT1), and the lower plenum pressure (PT2) were recorded. Both pressures of PT1 and PT2 are measured by a piezo electric pressure transducer. Datasets of pressure are collected for a period of 40 sec with a sampling frequency of 1 kHz. Since one of the aims of the experiments is to examine the bubble characteristics in the CCFL condition, visualization experiments were also carried out using a high-speed camera. The camera was fixed on a stand very close to the upper entry of the test tube to visualize both the bubble formation process and the behavior of the water. In the present experiments, pictures were taken at a speed of 250 frames per second and a shutter rate of 1/2000. After steady-state measurements were over, the air flow rate was progressively increased by small steps. These measurements and bubble observations were conducted at several air flow rates until the reversal of the liquid flow was initiated. Initiation of liquid flow reversal was observed by naked eye.

The two pressure transducers were calibrated using digital pressure gage before experiments. The air flow meter was

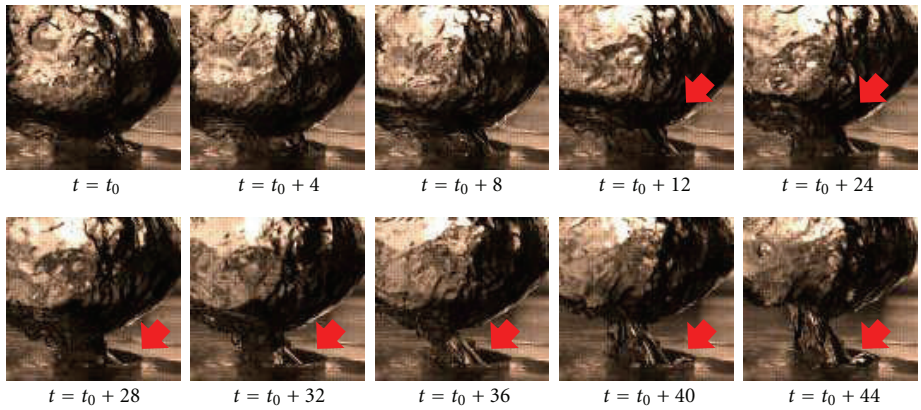

(a) Video images of bubble "neck" in the detachment process (tube diameter $D = 12$ mm, $j_g^{*0.5} = 0.61$, $H = 200$ mm)

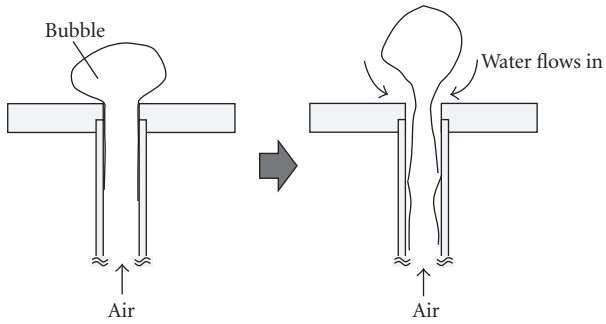

(b) Schematic of water flow at the upper entry

Figure 7: Video images of bubble "neck" at the upper entry of tube and sequence of water flow at the upper entry.

also calibrated using a dry-type gas flow meter. From these calibrations, the uncertainties of pressure measurements and air flow rate are ±5% and ±7%, respectively. The reproducibility and uncertainties of water flow rate was confirmed by repeating the measurements under the same air flow rate. From there measurements, the uncertainties of water flow rate are ±6%.

3. Experimental Results and Discussions

3.1. Effect of Tube Diameter. Figure 3 indicates relationship between a downward liquid flow and an upward gas flow rates. In the figure, the data are plotted in square terms of dimensionless superficial gas velocity j_g^* versus the corresponding dimensionless liquid superficial velocity j_l^*. The figure shows that, for both tubes, the slopes are almost linear throughout the entire range and can be fitted by straight lines by (1). It is clearly shown that the slopes of lines are affected by the tube diameter in the present countercurrent flow condition. The values of m and C obtained by fitting the present data with (1) were indicated in the figure.

Figure 4(a) shows typical time variations of pressure measured at the upper entry of the tube for the diameter of 12 mm. Here, the dimensionless gas velocity $j_g^{*0.5}$ was set at 0.88. As shown in this figure, there are four pressure fluctuation cycles ranging in peak height from 4 to 7 kPa. One of pressure fluctuation cycles is shown in Figure 4(b). Some of video images at the upper entry of the tube are shown in Figure 4(c) to illustrate this bubble cycle. The corresponding video images in Figure 4(c) are indicated as (1) to (8) in Figure 4(b). It can be seen that at the initial stage of bubble formation, the bubble size gradually increases with large pressure fluctuation. The bubble gradually changes with a hemispherical shape at the upper entry surface (Figure 4(c), (1) to (3)). As the bubble size increases, the buoyancy force is dominant, and then the bubble gradually became oblate spheroid (Figure 4(c), (4) to (6)) as it rises towards upward. At this stage, the pressure fluctuation gradually decreases. It should be noted that in Figure 4(c) (6), the "neck" can be seen in the bottom of the bubble.

Figures 5(a), 5(b), and 5(c) also show time variations of pressure and video images taken for the 20 mm tube diameter. The dimensionless gas velocity $j_g^{*0.5}$ was set at 0.68. As shown in Figure 5(a), the time variation of pressure fluctuation also consists of the fluctuation cycles. One of the fluctuation cycle is shown in Figure 5(b), and some of the corresponding video images are shown in Figure 5(c). As shown in Figure 5(c), the bubble appears to be more deformed and its size became larger than that of 12 mm tube diameter. Similar to the 12 mm diameter tube, at the

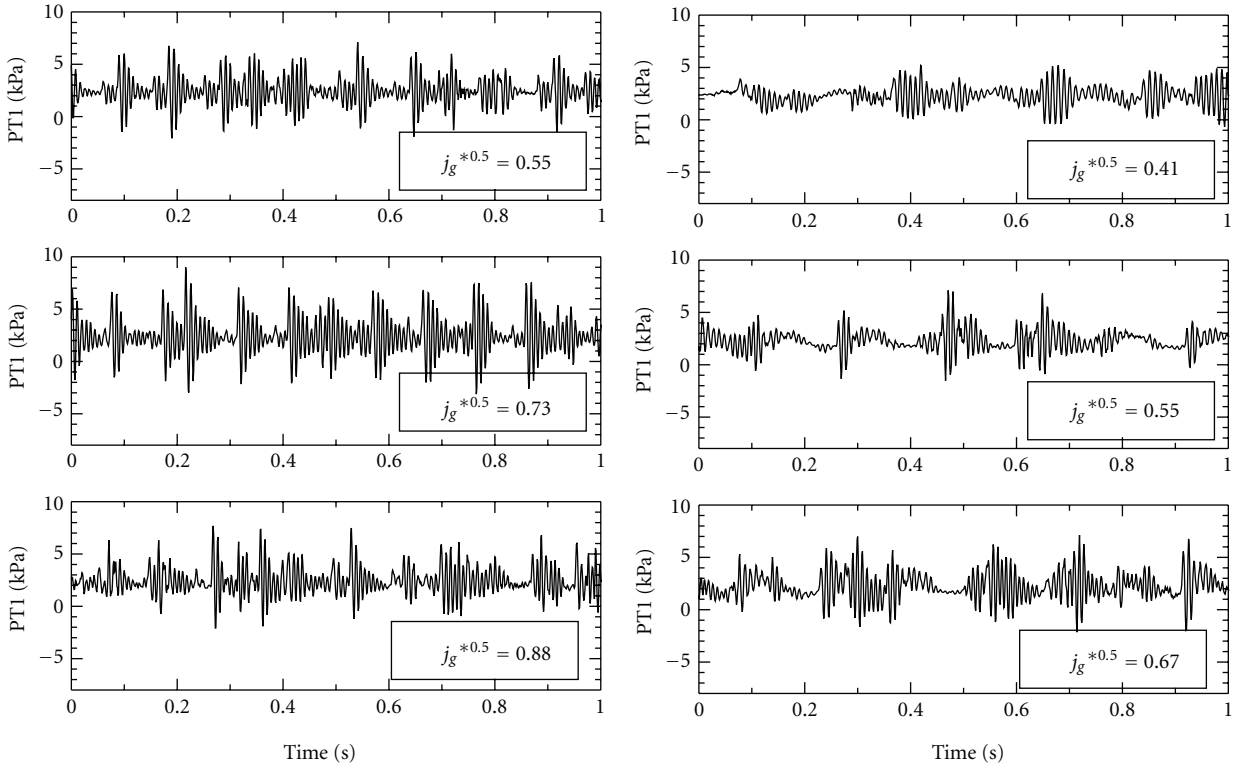

(a) Tube diameter: $D = 12$ mm

(b) Tube diameter: $D = 20$ mm

Figure 8: Typical time traces of pressure at the upper entry of the tube (PT1).

initial stage of the bubble growth (Figure 5(c) (1)–(5)), the pressure fluctuation is relatively large. As the bubble volume increases and it moves upward, the pressure fluctuation gradually decreased (Figure 5(c) (8)). As shown in the figure, the bubble clearly detached from the surface(Figure 5(c) (8)). This means that there is a discrete time interval between one bubble and next bubble formation. This discrete time interval, named a "waiting time," was observed only in the 20 mm diameter tube.

Typical video images including the waiting time are shown in Figure 6. As shown in Figure 6, the waiting time (indicated as (1) to (4) in Figure 6(b)) is characterized by the period in which no bubble is newly formed into the pool. It is noted that the water enters the tube in this waiting time between the bubble detachment and an initiation of next bubble formation. In addition, the waiting time was observed especially low air flow rate condition below $j_g^{*0.5} = 0.6$.

Above observations indicate the importance of relationship between the bubble formation and the behavior of the water in the upper plenum. Particularity, the bubble deformation during detachment process is important. Figure 7(a) includes the sequence of pictures showing "neck," where the bubble diameter gradually decreases at the tube entry. The time interval between two frames is 4 msec (1/250). Moreover, the water in the upper plenum continues to move downwards until next bubble will be formed at the upper entry. Sequence of this process is shown in Figure 7(b). When the gas bubble fully covers the tube diameter, the water cannot penetrate into the tube. However, as the bubble volume increased and the "neck" formed during detachment process, the water in the upper plenum can flows into the test tube.

Examples of the time variations of measured pressure at the location of the upper entry of the tube (PT1) are summarized in Figure 8. Although the measured data have similar time variations, the pressure of 12 mm diameter tube indicates larger fluctuations with a high frequency than that of 20 mm diameter tube. Typical power spectral densities (PSDs) of pressure fluctuations for the 12 mm diameter tube are shown in Figure 9 for three different values of air flow rates. The PSD data are corresponding to the locations of upper entry of the tube (PT1) and lower plenum (PT2), respectively. For the case of the upper entry of the tube, it appears that as increasing the gas flow rate, the peak of PSD is observed at frequencies between 13 and 15 Hz, while for the lower plenum pressure, this maximum corresponds to a frequencies between 5 and 11 Hz. The PSD of the pressure fluctuations measured in the 20 mm diameter tube is shown in Figure 10. For the larger tube diameter, the figure clearly shows sharp distinct peak both upper and the lower pressure fluctuations. Although the time variations of measured pressure shows similar trend, the calculated values of PSD are quite different. In particulary, the calculated "Power" of 20 mm diameter tube is much larger than that of 12 mm diameter tube. This fact suggests that the bubble

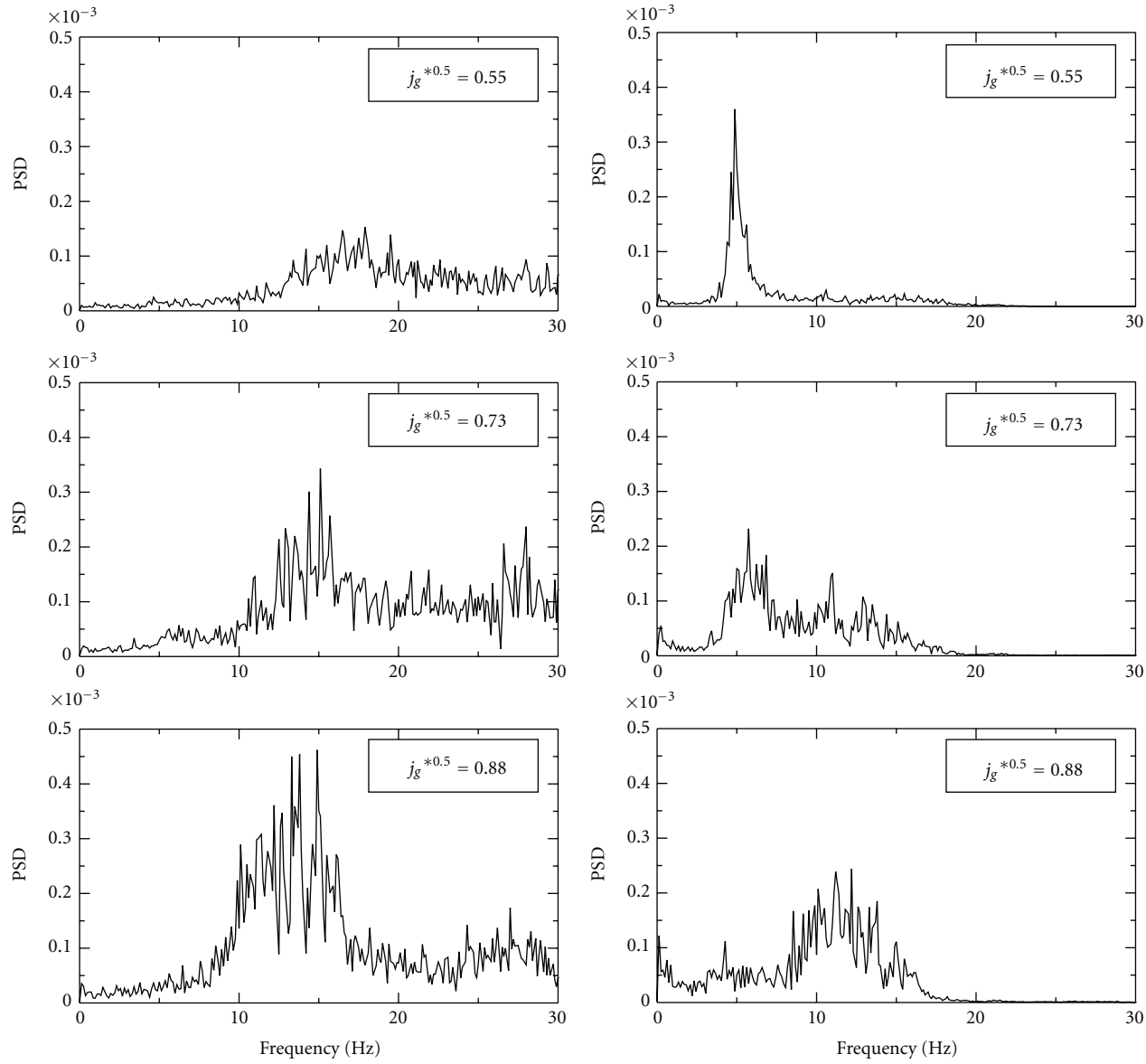

(a) Upper entry of the tube (PT1)

(b) Lower plenum (PT2)

Figure 9: Power spectrum density (PSD) of pressure fluctuations for various air flow rate (tube diameter, $D = 12$ mm).

formation cycle of 20 mm diameter tube is more repeatedly and periodically than that of 12 mm diameter tube.

3.2. Effect of Water Level in the Upper Plenum. In order to investigate the water level effect on the downward liquid flow rate in the CCFL condition, experiments are performed for three different water levels: 50, 100, and 200 mm, respectively. For the 12 mm diameter tube, relationship between dimensionless fluxes for three different water levels is shown in Figure 11(a). It seems that the water level effect on the liquid flow rate is small at high gas flow rate. It can be seen that although the parameter C in (1) is the same, the slope of the line slightly depends on water heights. On the other hand, the m and C are almost constant for the tube diameter of 20 mm as shown in Figure 11(b). This water level effect on downward liquid flow rate is found to occur only in the 12 mm diameter tube and not in 20 mm diameter tube. For the 20 mm diameter tube, since the bubble formation including the "waiting time" periodically occurs, the water in the upper plenum smoothly flows into the tube. Therefore, the downward liquid flow rate is not influenced by the water level in the upper plenum. On the other hand, for the 12 mm diameter tube, the downward liquid flow rate depends on the "neck" formation during bubble detachment process. Therefore, if the water level is small, the bubble reaches the free surface before the detachment occurs. Thus, the downward liquid flow rate for 12 diameter tube is affected by the water level in the upper plenum.

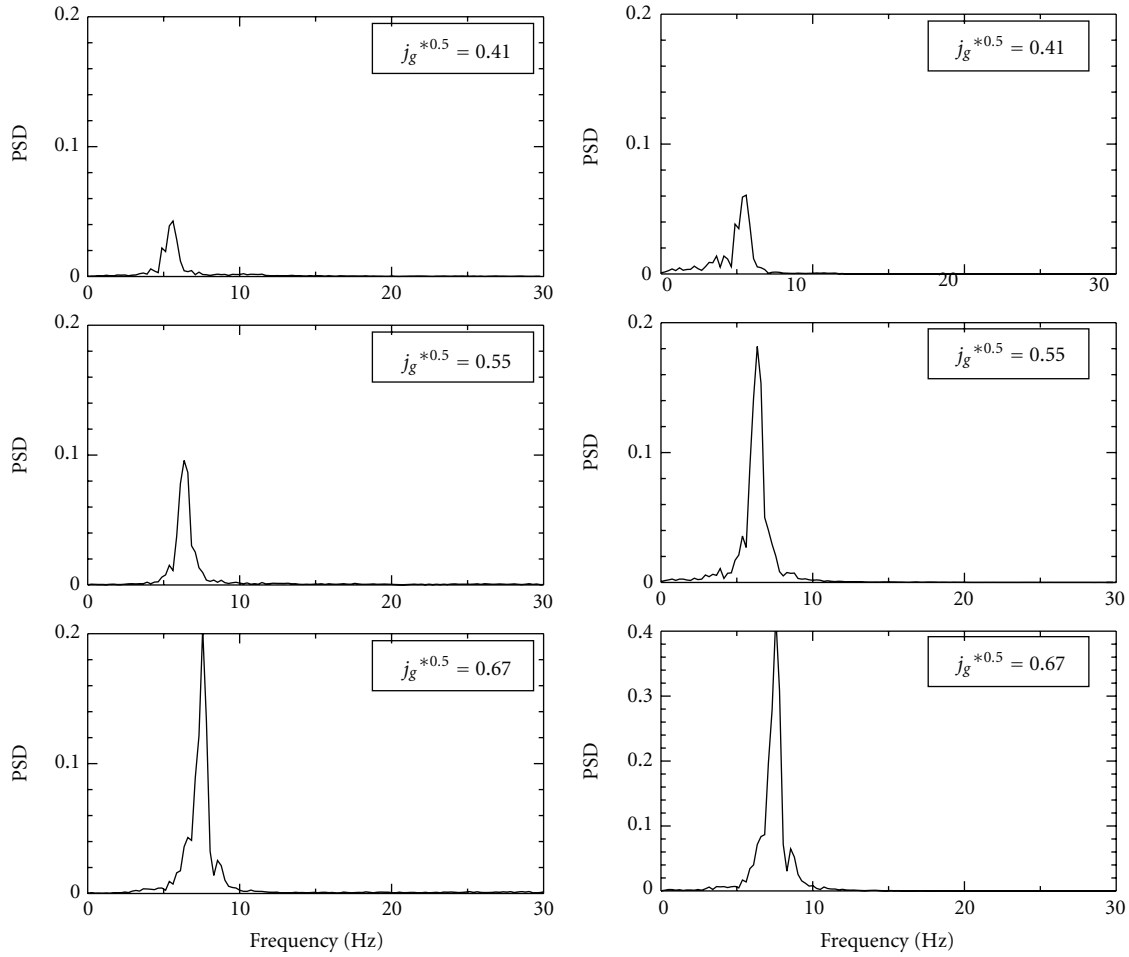

(a) Upper entry of the tube (PT1)

(b) Lower plenum (PT2)

Figure 10: Power spectrum density (PSD) of pressure fluctuations for various air flow rate (tube diameter, $D = 20$ mm).

The pressure difference and the downward liquid flow rate measured in the 12 mm tube diameter are plotted as a function of superficial air velocity in Figure 12(a). Here, the pressure difference indicates the difference of pressure between the upper entry of the tube (PT1) and the lower plenum pressure (PT2). The figures show that the pressure difference does not change appreciably, the downward flow rate decreases gradually as increasing the gas flow rate. Since the downward liquid flow rate depends on the bubble frequency at the upper entry of the tube, it gradually decreases as increasing the superficial air velocity. In addition, since the amount of downward liquid flow rate is small for 12 mm diameter tube, the liquid film in the tube is thin, and the pressure difference ΔP may not be influenced by the air superficial velocity.

The pressure difference and downward liquid flow rate measured in the 20 mm diameter tube is also presented in Figure 12(b). It is seen that for the 20 mm diameter tube, the pressure difference gradually increases as increasing the air flow rate. The downward liquid flow rate is almost inversely proportional to air superficial velocity. Since the bubble volume of the 20 mm tube diameter is much larger than that of the 12 mm tube diameter, the bubble detachment at the upper entry of the tube produces large pressure fluctuation in the lower plenum (PT2). Therefore, the dependence of ΔP on air superficial velocity is slightly different for two tube diameters.

Figures 13(a) and 13(b) show the power spectral density (PSD) measured in the 12 mm diameter tube for the upper entry of the tube and lower plenum, respectively. As shown in Figure 13(a), a distinct peak is not evident at the lowest air flow rate. However, as increasing the air flow rate, the peak gradually appears between 10 to 15 Hz. On the contrary, the PSD of the lower plenum indicates different tendency. When the air flow rate is relatively small, the frequency peak appears between 5 and 8 Hz. However, at the largest air flow rate, the peak is not clear except water height of 50 mm. The PSD for the 20 mm diameter tube is also shown in Figure 14 for the upper entry of the tube and the lower plenum, respectively. For this condition, it is apparent that the distinct peak clearly can be seen for all experimental conditions. The dominant

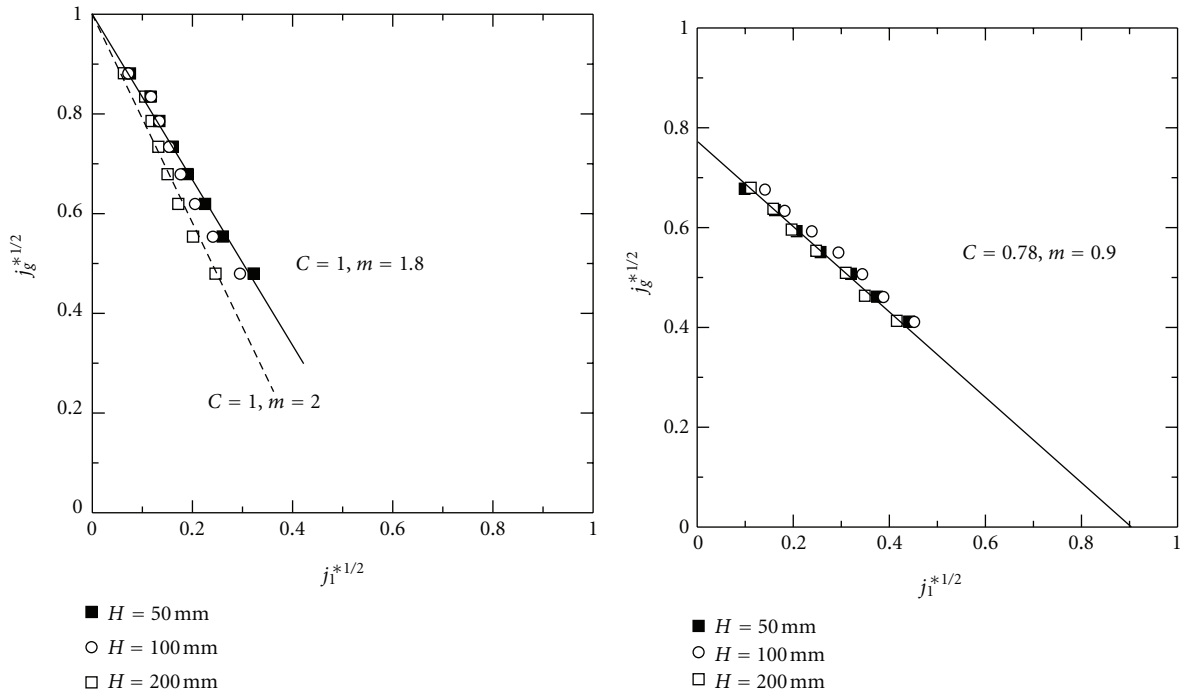

(a) $D = 12$ mm (b) $D = 20$ mm

Figure 11: Effect of water level on dimensionless liquid flow rate against gas flow rate in CCFL condition.

frequency is slightly dependent on the water height in the upper plenum.

Figure 15 shows the dominant frequency in the PSD as a function of gas flow rate for different three water levels. The dominant frequency was calculated using least-square method in the frequency ranges below 30 Hz. According to the visual observation, the bubble formation frequency, much less than 30 Hz, therefore, this frequency range was selected. As shown in Figure 15(a), the dominant frequency in the 12 mm diameter tube decreases with increasing gas flow rate. On the contrary, as shown in Figure 15(b), the dominant frequency of 20 mm diameter tube increases as increasing the gas flow rate.

Figures 15(a) and 15(b) show that the dependence of dominant frequency on the gas flow rate is quite different for two diameter tubes. One of the reasons of this difference depends on the bubble formation cycle. As shown in Figures 5, 6, and 14, the single bubble was periodically formed for 20 mm diameter tube. On the contrary, for the 12 mm diameter tube, the bubble detachment process is very complicated and two or three bubbles coalescence was observed at the upper entry as shown in Figure 4(c) (8). It should be noted that the bubble flow pattern at the upper entry of the tube becomes more complicated one as increasing the gas flow rate.

3.3. Comparison of Bubble Frequency Data with the Prediction. In the present experiment, visual images show that the bubble formation, expansion, and its detachment from the upper entry of the tube apparently occurred repeatedly. It is well known that there are number of correlations to predict the bubble formation from the orifice. Since the bubble formation significantly affects the downward liquid flow rate in the CCFL condition, the present results were compared with the proposed bubble formation correlations.

Davidson and Shuler [8] proposed the theoretical model for the periodic formation of bubbles due to the flow of gas into an inviscid liquid. The bubble formation expansion by an air injection into a pool might be controlled by forces of buoyancy, inertia due to momentum change of the liquid surrounding the bubble, drag, and surface tension. For a constant pressure condition, bubble is expanded very rapidly just after the pressure exceeds the required value for the bubble to advance into a pool. Therefore, the buoyancy and liquid inertia forces were considered in the force balance.

The buoyancy force is

$$\left(\rho_l - \rho_g\right) g V_B \approx \rho_l g V_B, \tag{4}$$

where, V_B means the bubble volume and the liquid inertia force is

$$\frac{d}{dt}\left(m\frac{ds}{dt}\right), \tag{5}$$

where s is a distance from the air injection point to a gravity center of the bubble and m is a virtual mass added to the bubble by the surrounding fluid and assumed as follows [8]:

$$m = \frac{11}{16}\rho_l V_B. \tag{6}$$

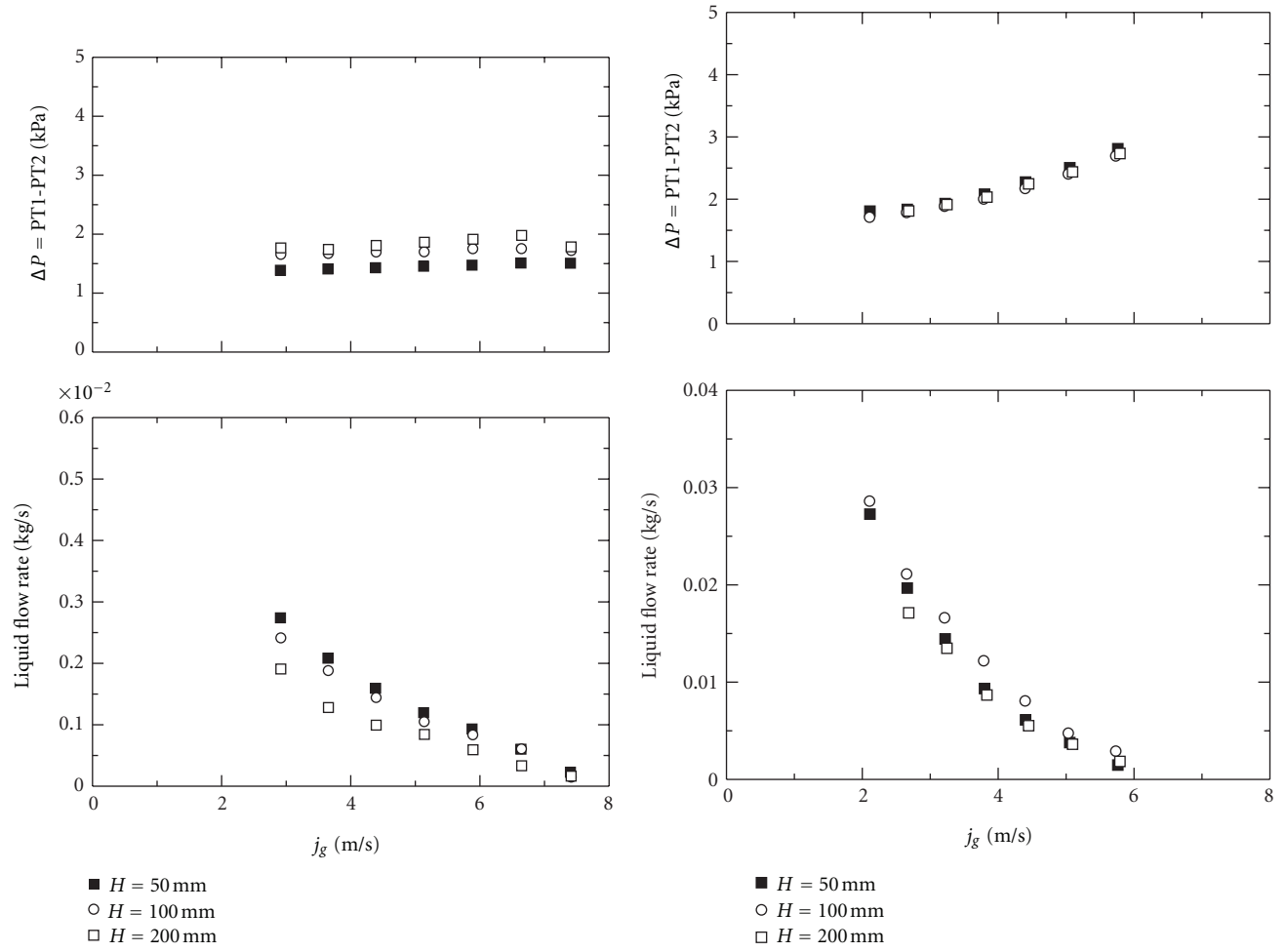

Figure 12: Variation of the pressure difference (PT1-PT2) and the downward liquid flow rate with superficial air flow rate for difference water level and tube diameter.

The force balance gives

$$\rho_l g V_B = \frac{d}{dt}\left(\frac{11}{16}\rho_l V_B \frac{ds}{dt}\right). \tag{7}$$

If the air flow rate is constant Q_g, then the bubble volume is given by

$$V_B = Q_g t. \tag{8}$$

Integrating the above differential equation using the initial condition that $s = 0$ and $ds/dt = 0$ when $t = 0$, the following equation for the bubble volume is obtained:

$$V_B = 1.378 Q_g^{6/5} g^{-3/5}. \tag{9}$$

Among the other bubble formation correlations, Wraith [9] proposed a simple two-stage model a plate orifice submerged in an inviscid liquid, for high gas flow rate. In his model, the first stage corresponds to the growth of a hemispherical bubble pressed to the plate by the inertial force. When the buoyancy force becomes dominant, a second stage develops and the bubble formation is dealt with as a virtual mass problem like Davidson model. The solution for the two-stage growth model by Wraith gives the following correlation:

$$V_B = 1.090 Q_g^{6/5} g^{-3/5}. \tag{10}$$

It is interesting to note that these two models take the following form:

$$V_B = k Q_g^{6/5} g^{-3/5}, \tag{11}$$

where k is the constant coefficient.

The data obtained in the present study are compared in Figures 16(a) and 16(b) with the correlations of Davidson (7) and of Wraith (8). In order to compare the experimental results with the correlations, an average volume of one detached bubble was calculated by following equation:

$$V_B = \frac{Q_g}{f}, \tag{12}$$

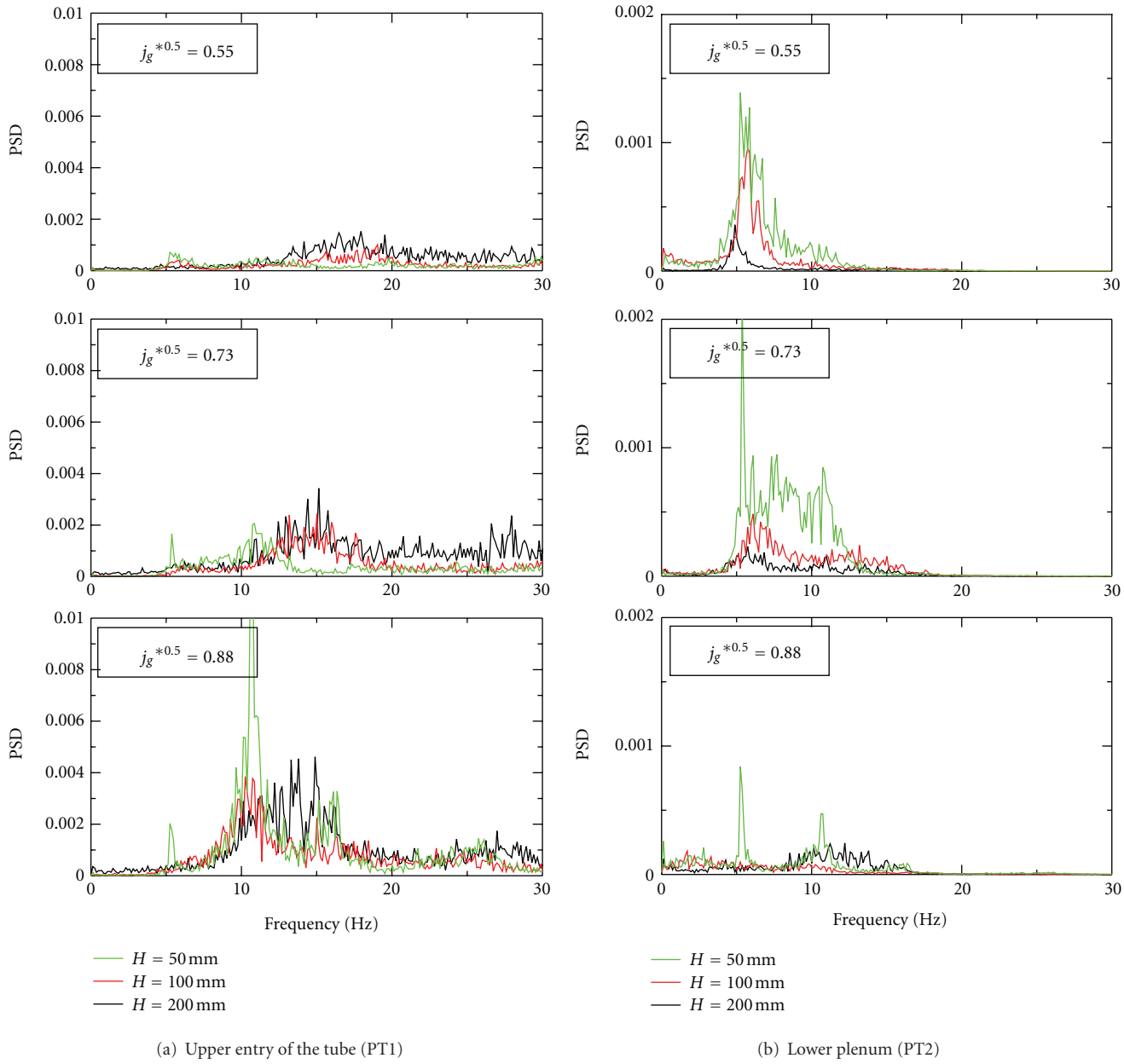

(a) Upper entry of the tube (PT1)

(b) Lower plenum (PT2)

Figure 13: Power spectrum density (PSD) of pressure fluctuations for various air flow rates and water levels (tube diameter $D = 12$ mm).

where Q_g is the gas volumetric flow rate (cm^3) and f is the dominant frequency of the pressure fluctuations in the upper entry of the tube. The figure shows that mea-sured bubble volumes increases monotonically with the gas flow rate. Figure 16(a) shows the data for 12 mm diameter tube, and it can be seen that Wraith correlation by (10) agree: with the data for water level of 100 mm and 200 mm. However, as shown in the figure, (9) and (10) slightly underestimate the data of the water level of 50 mm. The data in the 20 mm diameter tube are compared in Figure 16(b); the slope of the analytical relation is a little larger than the measured one and at a lower gas flow rate it underestimates the bubble volume and that the data gradually approach the analytical relation, and at a larger gas flow rate, the analysis can give a fairly good prediction. The calculated dominant frequency of 20 mm diameter tube includes the bubble "waiting time" in which no bubbles are formed at the tube entry. Therefore, in order to evaluate the detached bubble volume more precisely, the influence of bubble waiting time on pressure fluctuation should be well understood.

4. Conclusions

An experimental study has been conducted to study the Counter Current Flow Limitation in the tubes of 12 mm and

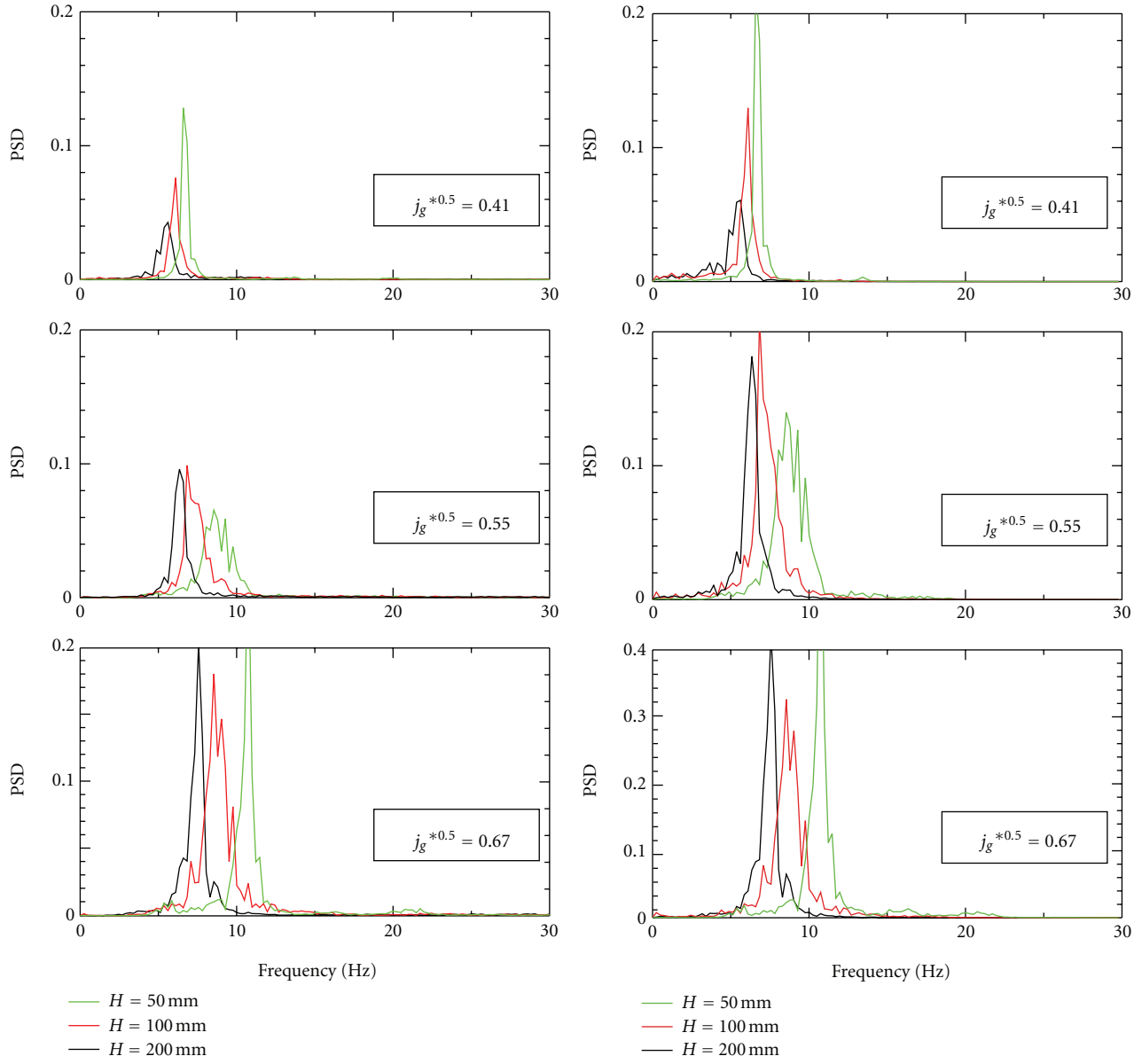

(a) Upper entry of the tube (PT1)

(b) Lower plenum (PT2)

Figure 14: Power spectrum density (PSD) of pressure fluctuations for various air flow rates and water levels (tube diameter $D = 20$ mm).

20 mm diameter. The pressures at the upper entry of the tube, lower plenum, and downward falling liquid flow rate were measured over a range of liquid and air flow rates. In addition, the relationship between the downward liquid flow and behaviors of bubbles purged into the liquid pool in the CCFL condition was also investigated using high-speed video camera. The following conclusions were made.

(1) The CCFL superficial velocities of gas and liquid obtained in the present experiments for two different diameter tubes are predicted well by correlation of Wallis. The water level in the upper plenum slightly affects the slope of the curve for the 12 mm i.d. tube, especially at low gas flow rate. On the other hand, for the 20 mm i.d. diameter tube, the slope of the curve is not affected by the water depth in the upper plenum.

(2) The "bubble one cycle" at the upper entry of the tube corresponds to characteristic one pressure fluctuation cycle. In this bubble cycle, the bubble growth, coalescence, and detachment at the upper entry of the tube were clearly observed. The bubble detachment process is quite different for two diameter tubes. For the 12 mm diameter tube, the formation of the "neck" during bubble detachment is important for evaluating the downward liquid flow rate. On the contrary, for the 20 mm diameter tube, a "waiting time" in which no bubble is observed at the upper entry is important to evaluate the downward liquid flow rate.

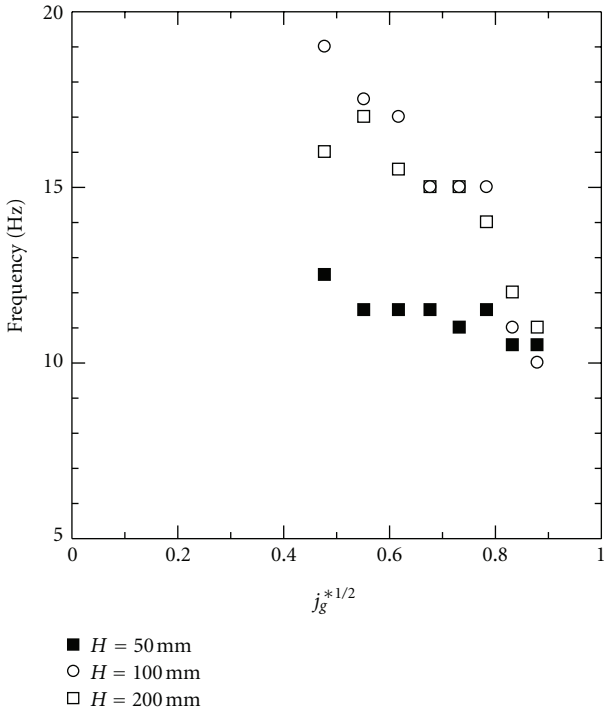

(a) $D = 12$ mm

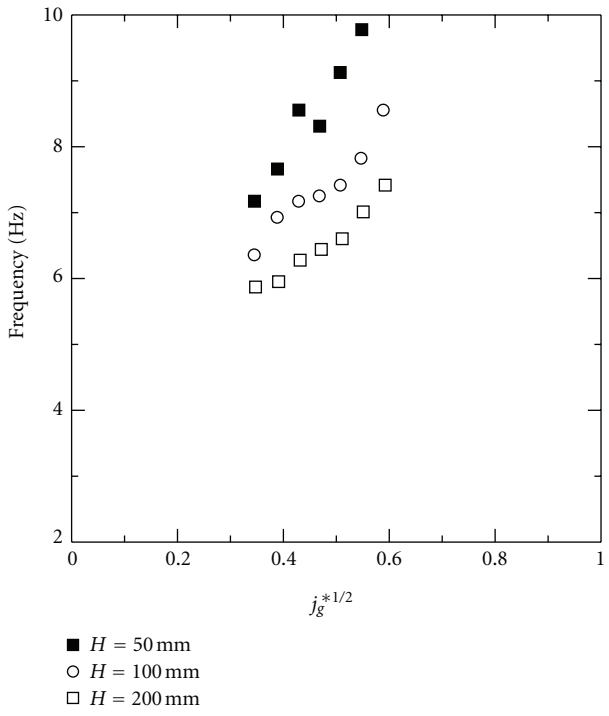

(b) $D = 20$ mm

Figure 15: Relationship between dominant frequency of bubble formation and dimensionless air superficial velocity.

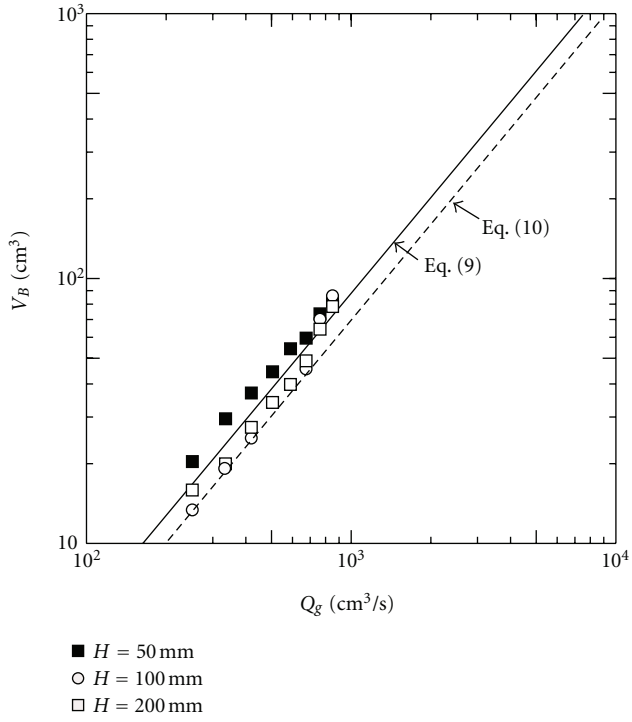

(a) $D = 12$ mm

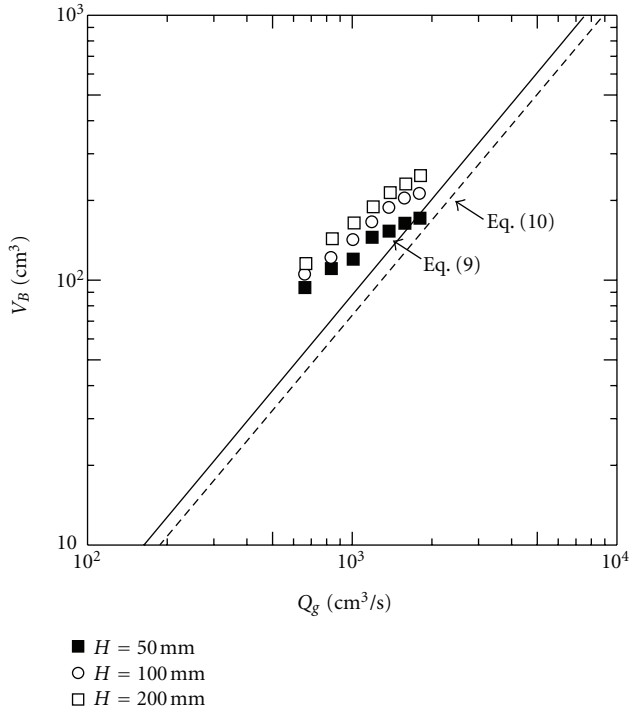

(b) $D = 20$ mm

Figure 16: Comparison of present experimental data with proposed correlations for bubble formation.

(3) The detaching bubble volume is predicted well by Davidson and Wraith correlations for 12 mm diameter tube. However, for the tube diameter of 20 mm, the correlations underestimate the experimental bubble volume especially at the low air flow rate. In the present experiments, the data for 20 mm diameter tube include the effect of "waiting time," therefore, the calculated bubble frequency may be affected by this characteristic period. It should be noted that the waiting time may be a favorable period for a liquid introduction into the test tube from the upper plenum.

References

[1] G. B. Wallis, *One-Dimensional Two-Phase Flow*, McGraw Hill, NewYork, NY, USA, 1969.

[2] H. J. Richter, "Flooding in tubes and annuli," *International Journal of Multiphase Flow*, vol. 7, no. 6, pp. 647–658, 1981.

[3] H. C. No and J. H. Jeong, "Flooding correlation based on the concept of hyperbolicity breaking in a vertical annular flow," *Nuclear Engineering and Design*, vol. 166, no. 2, pp. 249–258, 1996.

[4] F. Kaminaga, K. Matsumura, A. Ouchi, and Y. Shibata, "Study on relationship between rising gas bubble and falling liquid flow in CCFL condition," in *Proceedings of the 6th International Conference on Nuclear Engineering (ICONE '98)*, 1998.

[5] H. Imura, H. Kusuda, and S. Funatsu, "Flooding velocity in a counter-current annular two-phase flow," *Chemical Engineering Science*, vol. 32, no. 1, pp. 79–87, 1977.

[6] D. Bharathan and G. B. Wallis, "Air-water countercurrent annular flow," *International Journal of Multiphase Flow*, vol. 9, no. 4, pp. 349–366, 1983.

[7] D. C. Lu, N. S. Liao, and K. H. Wu, "Experimental investigation of counter-current steam-water flooding in a vertical circular pipe," in *Proceedings of the ASME-JSME Thermal Engineering Joint Conference*, vol. 1, pp. 243–249, Honolulu, Hawaii, USA, 1983.

[8] J. F. Davidson and B. O. G. Shuler, "Bubble formation at an orifice in an inviscid liquid," *Transactions of the Institute of Chemical Engineers*, vol. 38, pp. 335–342, 1960.

[9] A. E. Wraith, "Two stage bubble growth at a submerged plate orifice," *Chemical Engineering Science*, vol. 26, no. 10, pp. 1659–1671, 1971.